Chemical Science

We have presented the Graphical Abstract text and image for your article below. This brief summary of your work will appear in the contents pages of the issue in which your article appears.
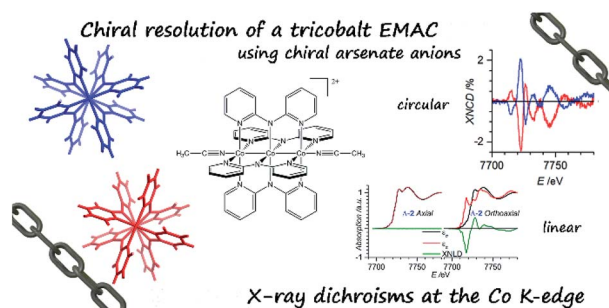
1

Enantiomeric resolution and X-ray optical activity of a tricobalt extended metal atom chain

Anandi Srinivasan, Miguel Cortijo, Vladimir Bulicanu, Ahmad Naim, Rodolphe Clérac, Philippe Sainctavit,* Andrei Rogalev, Fabrice Wilhelm, Patrick Rosa and Elizabeth A. Hillard*

Chiral metal chains at the edge. Enantiopure single crystals of extended metal atom chains display exceptionally large optical X-ray dichroisms at the Co K-edge.

Please check this proof carefully. **Our staff will not read it in detail after you have returned it.**

Proof corrections must be returned as a single set of corrections, approved by all co-authors. No further corrections can be made after you have submitted your proof corrections as we will publish your article online as soon as possible after they are received.

Please ensure that:

- The spelling and format of all author names and affiliations are checked carefully. Names will be indexed and cited as shown on the proof, so these must be correct.
- Any funding bodies have been acknowledged appropriately.
- All of the editor's queries are answered.
- Any necessary attachments, such as updated images or ESI files, are provided.

Translation errors between word-processor files and typesetting systems can occur so the whole proof needs to be read. Please pay particular attention to: tables; equations; numerical data; figures and graphics; and references.

Please send your corrections preferably as a copy of the proof PDF with electronic notes attached or alternatively as a list of corrections – do not change the text within the PDF file or send a revised manuscript. Corrections at this stage should be minor and not involve extensive changes.

Please return your **final** corrections, where possible within **48 hours** of receipt, by e-mail to: chemicalscience@rsc.org. If you require more time, please notify us by email.

Funder information

Providing accurate funding information will enable us to help you comply with your funders' reporting mandates. Clear acknowledgement of funder support is an important consideration in funding evaluation and can increase your chances of securing funding in the future. We work closely with Crossref to make your research discoverable through the Funding Data search tool (http://search.crossref.org/funding).

Further information on how to acknowledge your funders can be found on our webpage (http://rsc.li/funding-info).

What is Funding Data?

Funding Data (http://www.crossref.org/fundingdata/) provides a reliable way to track the impact of the work that funders support. We collect funding information from our authors and match this information to funders listed in the Crossref Funder Registry. Once an article has been matched to its funders, it is discoverable through Crossref's search interface.

PubMed Central

Accurate funder information will also help us identify articles that are mandated to be deposited in PubMed Central (PMC) and deposit these on your behalf.

Providing funder information

We have combined the information you gave us on submission with the information in your acknowledgements. This will help ensure funding information is as complete as possible and matches funders listed in the Crossref Funder Registry. **Please check that the funder names and grant numbers in the table are correct.** This table will not be included in your final PDF but we will share the data with Crossref so that your article can be found *via* the Funding Data search tool.

Funder name	Funder ID (for RSC use only)	Award/grant/contract number
Agence Nationale de la Recherche	501100001665	ANR-11-JS07-013-01
H2020 Marie Skłodowska-Curie Actions	100010665	706556
Université de Bordeaux	501100006251	Unassigned
European Synchrotron Radiation Facility	501100001671	CH-4171, CH-4457, CH-5009
Centre National de la Recherche Scientifique	501100004794	Unassigned

If a funding organisation you included in your acknowledgements or on submission of your article is not currently listed in the registry it will not appear in the table above. We can only deposit data if funders are already listed in the Crossref Funder Registry, but we will pass all funding information on to Crossref so that additional funders can be included in future.

Researcher information

If any authors have ORCID or ResearcherID details that are not listed below, please provide these with your proof corrections.

Please check that the ORCID and ResearcherID details listed below have been assigned to the correct author. Authors should have their own unique ORCID iD and should not use another researcher's, as errors will delay publication.

Please also update your account on our online manuscript submission system to add your ORCID details, which will then be automatically included in all future submissions. See here for step-by-step instructions and more information on author identifiers.

First (given) name(s)	Last (family) name(s)	ResearcherID	ORCID
Anandi	Srinivasan		
Miguel	Cortijo		0000-0002-3970-0720
Vladimir	Bulicanu		
Ahmad	Naim		
Rodolphe	Clérac		0000-0001-5429-7418
Philippe	Sainctavit		
Andrei	Rogalev		
Fabrice	Wilhelm		
Patrick	Rosa	H-7576-2017	0000-0001-5670-2624
Elizabeth A.	Hillard		0000-0002-5149-0324

Queries for the attention of the authors

Editor's queries are marked on your proof like this **1**, **2**, etc. and for your convenience line numbers are indicated like this 5, 10, 15,

Please ensure that all queries are answered when returning your proof corrections so that publication of your article is not delayed.

Query Reference	Query	Remarks
1	Funder details have been incorporated in the funder table using information provided in the article text. Please check that the funder information in the table is correct.	
2	Please check that the inserted CCDC numbers are correct.	
3	Please confirm that the spelling and format of all author names is correct. Names will be indexed and cited as shown on the proof, so these must be correct. No late corrections can be made.	
4	Please check that address *e* has been displayed correctly.	
5	The caption to Fig. 5 refers to parts (a) and (b) but the image as supplied does not contain parts labelled (a) and (b). Would you like to modify the caption or resupply the artwork (preferably as a TIF file at 600 dots per inch)?	
6	Ref. 19: Can this reference be updated? Please supply details to allow readers to access the reference (for references where page numbers are not yet known, please supply the DOI).	

Enantiomeric resolution and X-ray optical activity of a tricobalt extended metal atom chain†

Anandi Srinivasan,‡[ab] Miguel Cortijo, [ID] ‡[abcd] Vladimir Bulicanu,[ab] Ahmad Naim,[cd] Rodolphe Clérac, [ID] [ab] Philippe Sainctavit,*[e] Andrei Rogalev,[f] Fabrice Wilhelm,[f] Patrick Rosa [ID] [cd] and Elizabeth A. Hillard [ID] *[ab]

A simple procedure based on anion exchange was employed for the enantiomeric resolution of the extended metal atom chain (EMAC) [Co$_3$(dpa)$_4$(MeCN)$_2$]$^{2+}$. Use of the chiral salt (NBu$_4$)$_2$[As$_2$(tartrate)$_2$], (Λ-1 or Δ-1), resulted in the selective crystallization of the EMAC enantiomers as [Δ-Co$_3$(dpa)$_4$(MeCN)$_2$](NBu$_4$)$_2$[Λ-As$_2$(tartarte)$_2$]$_2$, (Δ-2) and [Λ-Co$_3$(dpa)$_4$(MeCN)$_2$](NBu$_4$)$_2$[Δ-As$_2$(tartrate)$_2$]$_2$ (Λ-2), respectively, in the P42$_1$2 space group, whereas a racemic mixture of 1 yielded [Co$_3$(dpa)$_4$(MeCN)$_2$][As$_2$(tartrate)$_2$]·2MeCN (rac-3), which crystallized in the C2/c space group. The local electronic and magnetic structure of the EMAC enantiomers was studied, exploiting a variety of dichroisms in single crystals. A strong linear dichroism at the Co K-edge was observed in the orthoaxial configuration, whereas it vanished in the axial orientation, thus spectroscopically confirming the D$_4$ crystal symmetry. Compounds Δ-2 and Λ-2 are shown to be enantiopure materials as evidenced by mirror-image natural circular dichroism spectra in the UV/vis in solution and in the X-ray range at the Co K-edge in single crystals. The surprising absence of detectable X-ray magnetic circular dichroism or X-ray magnetochiral dichroism signals at the Co K-edge, even at low temperature (3 K) and a high magnetic field (17 T), is ascribed to a strongly delocalized spin density on the tricobalt core.

Introduction

Extended Metal Atom Chains (EMACs) are a fascinating class of linear polynuclear coordination complexes, which have served as a rich playing field for the study of metal–metal bonding, magnetism and electrical conductivity.[1] In addition, most EMACs demonstrate helicoidal chirality arising from steric hindrance between the protons in the 3-position of the pyridine groups (Chart 1). These complexes almost exclusively crystallize as racemates, and chiral resolution has been accomplished in only a few isolated cases. For example, spontaneous resolution afforded crystals of homochiral

[Co$_3$(dpa)$_4$(MeCN)$_2$](PF$_6$)$_2$·MeCN·2Et$_2$O (where dpa = the anion of 2,2′-dipyridylamine), but only as a minor product.[2] These crystals were then painstakingly separated using X-ray diffraction to determine the handedness of each crystal, in order to then obtain circular dichroism measurements on an enantiopure sample. In another study, homochiral samples of a mixture of [Ni$_3$(dpa)$_4$Cl$_2$] and [Ni$_3$(dpa)$_4$ClOH] were obtained by chromatographic separation on a chiral stationary phase, while the cobalt and chromium analogues were unstable to chromatography.[3] More recently, naphthyridine ligands

^{a}CNRS, CRPP, UPR 8641, F-33600 Pessac, France. E-mail: hillard@crpp-bordeaux.cnrs.fr

^{b}Univ. Bordeaux, CRPP, UPR 8641, F-33600 Pessac, France

^{c}CNRS, ICMCB, UPR 9048, F-33600 Pessac, France

^{d}Univ. Bordeaux, ICMCB, UPR 9048, F-33600 Pessac, France

^{e}IMPMC, Université Pierre et Marie Curie, Institut de Recherche sur le Développement, Muséum National d'Histoire Naturelle, UMR CNRS 7590, 4 Place Jussieu, F-75252 Paris Cedex 05, France. E-mail: Philippe.Sainctavit@impmc.upmc.fr

^{f}European Synchrotron Radiation Facility (ESRF), F-38043 Grenoble, France

† Electronic supplementary information (ESI) available: Bond distances and angles for 2 and 3, thermal ellipsoid plots, packing diagrams, magnetization curves, thermogravimetric analysis, and additional XNCD and XMCD plots and CD spectra. CCDC 1574514–1574516 and 1588703. For ESI and crystallographic data in CIF or other electronic format see DOI: 10.1039/c7sc04131d
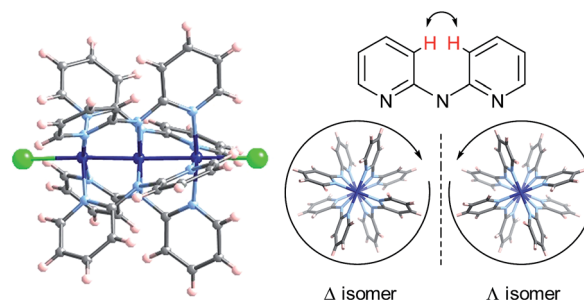
‡ Both authors contributed equally to this work.

Chart 1 (Left) Crystallographic model of [Co$_3$(dpa)$_4$Cl$_2$]; cobalt (dark blue), nitrogen (pale blue), chloride (green), carbon (gray), hydrogen (pink). (Right) Helicoidal wrapping of the dpa⁻ ligands; arrow indicates H-atom repulsions.

incorporating a chiral camphorsulfonyl group were conceived for the enantiopure synthesis of Ni_5 chains.[4]

The helicoidal chirality found in EMACs has several interesting features. UV/vis circular dichroism and polarimetry studies showed that the above-mentioned enantiomers of tricobalt, trinickel and pentanickel EMACs do not interconvert in solution, which is rather unusual for labile first-row transition metal complexes. This can be ascribed to a high energy barrier to racemization engendered by the polynuclear helix. Moreover, the optical activity for an acetonitrile solution of the mixture of nickel EMACs obtained by chromatography was found to be remarkably high, with a specific rotation of $[\alpha]_D^{22} \approx \pm 5000$ deg mL g^{-1} dm^{-1}.[3b] This value is on the same order of magnitude as that of the helicenes, the current record-holders for high specific rotation.[5]

Natural circular dichroism, first observed in 1895 by Aimé Cotton, is one of the most powerful tools for obtaining stereochemical information. Circular dichroism measurements have been only recently extended to X-ray absorption spectroscopy, which is inherently element selective. It was first achieved for X-ray magnetic circular dichroism (XMCD), which has become a workhorse technique for the exploration of the magnetic properties of absorbing atoms in magnetic materials. The first observation of X-ray Natural Circular Dichroism (XNCD) was made in 1998 on single crystals of α-$LiIO_3$ and $Na_3[Nd(digly)_3]\cdot$ $2NaBF_4\cdot6H_2O$.[6] Since then, a few other molecular systems have been studied, such as $[Co(en)_3Cl_3]\cdot NaCl\cdot6H_2O$ and the 1D coordination polymers $[Co(hfac)_2NITPhOMe]_\infty$ and $[Ln(Hnic)(nic)_2(NO_3)]_\infty$.[7] Even though it is still in its infancy, this spectroscopy appears to be a very sensitive probe of the chiral molecular environment around the absorbing atom. An important aspect of XNCD originates from a not well-known electric dipole-electric quadrupole mechanism that exists only in oriented samples. Moreover, it can only be observed in crystals belonging to one of 13 noncentrosymmetric crystal point groups.[8] Unfortunately, the electric dipole-magnetic dipole mechanism that is dominant in UV/vis natural circular dichroism, and which is observable in isotropic chiral media, vanishes in core-level X-ray spectroscopy. From this perspective, a related phenomenon, X-ray magnetochiral dichroism (XMχD), i.e. the propensity of chiral paramagnetic systems to exhibit a differential absorption of unpolarized light in the presence of a magnetic field is more appealing. This peculiar type of dichroism is due to orbital toroidal currents, which are relevant to many phenomena, ranging from multiferroicity to superconductivity. In the X-ray range, this effect has been unambiguously demonstrated in only two cases: in chromium oxide,[9] and more recently in $[Co(hfac)_2NITPhOMe]_\infty$.[7b] In addition to these dichroic effects, there exists also X-ray natural linear dichroism (XNLD), which directly measures the anisotropy of the electronic states of an absorbing atom.

Due to the attractive optical[3b] and magnetic properties[1] of EMACs, a general method for their enantiomeric resolution is highly desirable. In the present investigation, we have chosen to study tricobalt complexes supported by 2,2′-dipyridylamine ligands, not only due to their preparative ease and air-stability in the solid state, but also for their interesting magnetic

properties. Indeed, the electronic structure of tricobalt EMACs has been extensively studied, primarily due to the observation that several $[Co_3(dpa)_4X_2]$ derivatives display a temperature-induced $S = 1/2$ to $3/2$ spin-crossover (SCO).[1c,10] DFT calculations reveal that, in the ground state, one unpaired electron is delocalized over three equidistant cobalt centers in a metal-based σ_{nb} molecular orbital.[11] It is thought that SCO can then proceed by two different mechanisms, characterized by the retention or loss of the symmetry in the $\{Co_3\}$ core.[1,12]

Our synthetic approach takes advantage of the dicationic character of $[Co_3(dpa)_4(MeCN)_2]^{2+}$,[2] which permitted the selective precipitation of each of the enantiomers in association with an enantiopure chiral anion. As this method involves a straightforward anion exchange reaction, it is not necessary to rely on serendipity or to synthesize chiral ligands. For this work, we have chosen a pair of chiral arsenyl dianions, based on inexpensive and easily available tartaric acid.[13] Such D_2-symmetric As(III), as well as Sb(III), tartrate adducts have been widely used in chiral HPLC separations[14] and enantiopure crystallization[15] of metal complexes, and different mechanistic explanations for the chiral recognition of octahedral metal complexes have been proposed.[16] It is worth mentioning that potassium antimonyl tartrate is commercially available, but its low solubility in organic solvents precluded its use.

We present here results on the use of the lipophilic arsenyl tartrate salt, $(NBu_4)_2[As_2(tartrate)_2]$ (Δ-1 and Λ-1) in the resolution of $[Co_3(dpa)_4(MeCN)_2]^{2+}$ enantiomers. Chiral compounds so-obtained were optically, structurally and magnetically characterized and were found display a space group and a magnetic ground state compatible with the demonstration of X-ray natural and magnetochiral optical activity. Results of thorough polarization dependent X-ray spectroscopic studies performed at the Co K-edge reveal large XNCD and XNLD signals, but only vanishingly small XMCD and XMχD signals, likely due to the strongly delocalized nature of the magnetization on the tricobalt core.

Results and discussion

Synthesis and characterization

The tricobalt EMAC salt $[Co_3(dpa)_4(MeCN)_2](BF_4)_2$ was formed in situ by stirring an acetonitrile solution of $[Co_3(dpa)_4Cl_2]$[17] and 2 eq. of $AgBF_4$ for several hours. After filtration to remove AgCl, 1 eq. of Δ-1 or Λ-1 dissolved in MeCN was added to the filtrate and stirred for 1 h, yielding a deep green precipitate. The solid was isolated by filtration and re-dissolved in MeCN. Vapor ether diffusion into the acetonitrile solutions gave green plates (fast crystallization) and/or blocks (slow crystallization) of $[Δ-Co_3(dpa)_4(MeCN)_2](NBu_4)_2[Δ-As_2(tartrate)_2]_2$ solvent, (Δ-2), or $[Λ-Co_3(dpa)_4(MeCN)_2](NBu_4)_2[Δ-As_2(tartrate)_2]_2$ solvent, (Λ-2), after 2 days in ca. 40% yield. This yield is quite satisfactory, considering a maximum yield of 50%, given that the starting $[Co_3(dpa)_4(MeCN)_2](BF_4)_2$ is racemic and the enantiomers are not expected to interconvert in acetonitrile.[2] $[rac-Co_3(dpa)_4(MeCN)_2][As_2(tartrate)_2]\cdot2MeCN$ (rac-3) was also obtained by a similar reaction, using a racemic mixture of

(NBu$_4$)$_2$[As$_2$(tartrate)$_2$] **1**, and crystallized directly from acetonitrile upon standing in 95% yield.

The stoichiometry of **2** is unexpected, the simplest formula being the binary salt [Co$_3$(dpa)$_4$(MeCN)$_2$][As$_2$(tartrate)$_2$]. Instead, the compounds consist of one cobalt complex, two tetrabutylammonium cations and two arsenate dianions. The unusual stoichiometry may be explained by the 2-fold excess of **1** used in this anion exchange protocol. However, when 0.5 eq. of Δ or Λ-(NBu$_4$)$_2$[As$_2$(tartrate)$_2$] was used, the resulting green precipitate could not be subsequently crystallized and powder diffraction indicated that the polycrystalline precipitate was not isostructural with **2** (Fig. S8†).

The crystal structures of Δ-**2** and Λ-**2** were successfully solved and refined in the non-centrosymmetric P42$_1$2 space group, with Flack parameters of −0.008(2) and −0.002(2), respectively (Table 1). The [Co$_3$(dpa)$_4$(MeCN)$_2$]$^{2+}$ moieties are parallel to one another and are arranged so that the metal axes lie along the c crystal direction (Fig. 1). The arsenyl tartrate anions nestle in the voids between the molecular layers, with distances of 3.22 and 3.11 Å between the CO$^−$ group of the arsenyl tartrate and the axial CH$_3$CN and one pyridyl group of the EMAC, respectively (Fig. S4†). Notably, [Δ-As$_2$(tartrate)$_2$]$^{2−}$ crystallizes exclusively with [Λ-Co$_3$(dpa)$_4$(MeCN)$_2$]$^{2+}$ and *vice versa*; here, the Δ and Λ notation refers to the handedness of the tricobalt helix. The Co–Co distances are identical, due to a 2-fold axis bisecting the central cobalt ion. Bond distances and angles are typical of the starting materials and show no unusual features (Tables S1 and S2†).

The electron density of the interstitial solvent molecules was highly diffuse and could not be satisfactorily modeled. Refinement of the structures with solvent molecules omitted gave values of R$_1$ (all data) = 0.0553 and 0.0591 for Δ-**2** and Λ-**2**, respectively. The Platon Squeeze procedure[18] calculated one void space per unit cell (Fig. S7†), accounting for 39% of the total unit cell volume and containing about 550 electrons. The electron count corresponds to approximately twelve
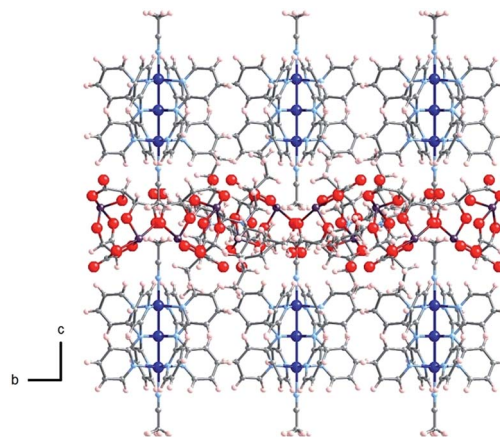

Fig. 1 Arrangement of **2** in the crystal viewed along the crystalline a axis; Co: dark blue, As: violet, O: red, N: light blue, C: gray, H: pink.

diethylether molecules per unit cell, or six ether molecules per formula unit (Z = 2). Successful re-refinement of the structure yielded R$_1$ (all data) = 0.0223 and 0.0353 for Δ-**2** and Λ-**2**, respectively. Thermogravimetric analysis (TGA) on a freshly filtered sample (Fig. S9†) showed a mass loss of approximately 11%, corresponding to *ca.* four molecules of diethylether per formula unit. Mass loss begins even at room temperature, accounting for the discrepancy between the number of solvent molecules estimated by X-ray diffraction and TGA. Solvent loss was also observed in the loss of crystallinity during attempted data collection at 280 K. As the void space is continuous in the ab plane, the solvent is not only highly mobile within the crystal, but can easily escape the crystal as well.

Compound *rac*-**3** crystallizes in the centrosymmetric C2/c space group and contains both enantiomers of the cations and anions. The Δ and Λ forms are segregated and contrary to the heterochiral interactions seen in Δ-**2** and Λ-**2**, anions and cations of the same chirality associate with each other in **3**

Table 1 Crystallographic data for Δ-**2**, Λ-**2** and *rac*-**3**

	Δ-**2**	Λ-**2**	*rac*-**3**
T/K	120	120	120
Empirical formula[a]	C$_{92}$H$_{118}$As$_4$Co$_3$N$_{16}$O$_{24}$		C$_{56}$H$_{48}$As$_2$Co$_3$N$_{16}$O$_{12}$
fw	2308.49		1463.73
Space group	P42$_1$2 (#90)		C2/c (#15)
a/Å	20.6481(10)	20.6668(10)	17.794(4)
b/Å	20.6481(10)	20.6668(10)	19.121(4)
c/Å	16.8896(9)	16.8568(9)	19.042(4)
β/°	90	90	116.941(15)
V/Å^3	7200.8(8)	7199.8(8)	5776(2)
Z	2	2	4
d (calc., g cm^{-3})	1.065	1.065	1.683
μ (mm^{-1})	1.309	1.309	2.067
R indices (all data)	R$_1$[b] = 0.0223, wR$_2$[c] = 0.0512	R$_1$[b] = 0.0353, wR$_2$[c] = 0.0784	R$_1$[b] = 0.0324, wR$_2$[c] = 0.0693
GooF on F^2	1.070	1.052	1.061
Flack parameter	−0.008(2)	−0.002(2)	—

[a] Solvent molecules of crystallization are not included in the empirical formula. [b] $R_1 = \Sigma||F_o| - |F_c||/\Sigma|F_o|$. [c] $wR_2 = [\Sigma[w(F_o^2 - F_c^2)^2]/\Sigma[w(F_o^2)^2]]^{1/2}$, $w = 1/\sigma^2(F_o^2) + (aP)^2 + bP$, where $P = [\max(0 \text{ or } F_o^2) + 2(F_c^2)]/3$.

(Fig. S5†), with distances of 3.14 and 3.12 Å between the CO–As group and the axial CH_3CN and one pyridyl group of the EMAC, respectively.

The chirality of Δ-**2** and Λ-**2** was first confirmed by UV/vis circular dichroism spectroscopy in acetonitrile solution (Fig. 2). Between 250–650 nm, the spectra plotted as $\Delta\varepsilon$ *vs.* λ are similar, but *ca.* 4× more intense, to those reported by Cotton and coworkers for the spontaneously resolved $[Co_3(dpa)_4(MeCN)_2](PF_6)_2$ enantiomers,[2] although the ε *vs.* λ values in the absorption spectra were found to be similar. The arsenyl tartrate peaks below 250 mn are masked by the much more intense peaks from the $[Co_3(dpa)_4(MeCN)_2]^{2+}$ moiety in the same area.[19]

Given that the circular dichroism spectra were measured separately, yet exhibit the same amplitude with opposite sign, fast racemization in solution can be excluded. A CD spectrum on a MeCN solution of Δ-**2** was measured after preparation, and again after 8 days at r.t. No loss of the peak intensity was observed (ESI†). Finally, the potential for chemical manipulation of **2** without loss of enantiopurity was demonstrated by exchanging the arsenyl tartrate anions with PF_6^- anions on a sample of Δ-**2** (ESI†). Recrystallization from acetonitrile and diethyl ether yielded crystals of Δ-$[Co_3(dpa)_4(MeCN)_2](PF_6)_2$·$CH_3CN$·$Et_2O$, as previously obtained by Cotton *et al.* by spontaneous resolution.[2] Circular dichroism spectroscopy in MeCN of Δ-$[Co_3(dpa)_4(MeCN)_2](PF_6)_2$ revealed slightly less intense peaks compared to those of Δ-**2** (ESI†), and no evolution after 5 days (ESI†), demonstrating that the chirality of the compound is maintained in solution, even in the absence of chiral anions.

To investigate potential SCO properties in Δ-**2** and Λ-**2**, the magnetic susceptibility was evaluated between 1.85 and 320 K in a 0.1 T applied field (Fig. 3 and S10†). Both compounds show a constant χT product at about 0.50 cm^3 K mol^{-1} between 5 and 200 K, close to what is expected for an $S = 1/2$ system with $g = 2.4$ (0.54 cm^3 K mol^{-1}), typical of other trinuclear cobalt EMACs.[1c,2] Above 200 K, the χT product increases gradually, as the signature of an SCO process, which becomes irreversible above 320 K as a sign of decomposition involving most likely the loss of the interstitial solvent molecules. Low temperature magnetization curves plotted *vs.* HT^{-1}, were superimposable, and a fit of these data at 1.9 K to the $S = 1/2$ Brillouin function,
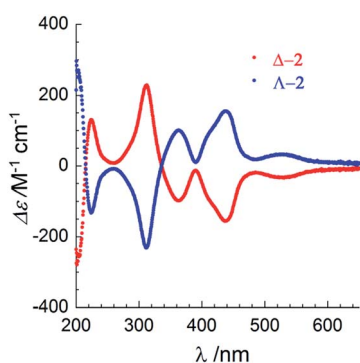

Fig. 3 Temperature dependence of the χT product for Δ-**2** (red) and Λ-**2** (blue) at 0.1 T, where χ is the magnetic susceptibility defined as M/H per mole of complex, with M being the magnetization and H the applied magnetic field.

gave $g = 2.3(1)$ for Δ-**2** and $g = 2.2(1)$ for Λ-**2** (Fig. S10†). The uncertainty in these two values is due to the inevitable doubt regarding the molecular weight of the samples because of interstitial solvent loss. Altogether, these results suggest that the delocalized ^2A_g state proposed by theory is the main contribution to electronic structure of **2** at all relevant temperatures.

X-ray absorption

To investigate the local chiral and magnetic properties of Δ-**2** and Λ-**2** we have performed thorough polarization dependent X-ray spectroscopy studies at the Co K-edge on single crystals. The experiments were carried out at the ID12 beamline of the European Synchrotron Radiation Facility, which is dedicated to such studies in the hard X-ray range. As Δ-**2** and Λ-**2** are chiral paramagnets, four different types of dichroisms in X-ray absorption are allowed by symmetry: X-ray Natural Linear Dichroism (XNLD) and X-ray Natural Circular Dichroism (XNCD), while application of an external magnetic field also permits X-ray Magnetic Circular Dichroism (XMCD), and X-ray Magneto-Chiral Dichroism (XMχD). If $\sigma_{H^+,L}$ represents the cross-section measured with left circularly polarized X-rays (L) in an external magnetic field parallel (H^+) to the X-ray propagation vector (and similar obvious definitions for right circular polarization and an antiparallel magnetic field), the three dichroic cross-sections making use of circular polarization are defined by

$$\sigma_{XMCD}(H) = \frac{[\sigma_{H^+,R} + \sigma_{H^-,L} - \sigma_{H^-,R} - \sigma_{H^+,L}]}{2} \quad (1)$$

$$\sigma_{XM\chi D}(H) = \frac{[\sigma_{H^+,R} + \sigma_{H^+,L} - \sigma_{H^-,R} - \sigma_{H^-,L}]}{2} \quad (2)$$

$$\sigma_{XNCD}(H) = \frac{[\sigma_{H^+,R} + \sigma_{H^-,R} - \sigma_{H^+,L} - \sigma_{H^-,L}]}{2} \quad (3)$$

It should be mentioned that $\sigma_{XNCD}(H)$, being independent of the magnetic field, is usually measured for $H = 0$. These three dichroic cross-sections are independent from each other and

Fig. 2 UV-visible circular dichroism spectra of Δ-**2** (red) and Λ-**2** (blue) between 200–650 nm in acetonitrile solution at room temperature.
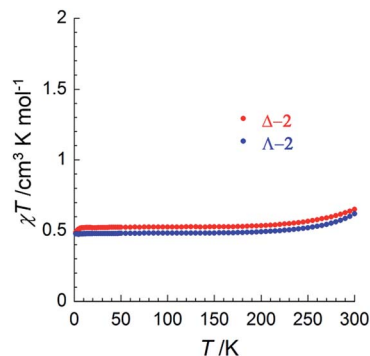
provide information on the electronic and magnetic structures of the element-specific absorbing atoms.

Our first experiment was an attempt to measure σ_{XMCD}. A single crystal of Δ-**2** was cooled down to 3 K and placed in the bore of a superconducting solenoid providing a magnetic field up to ±17 T. Absorption spectra were collected using circularly polarized X-rays where the propagation vector of the X-rays, as well as the magnetic field, were aligned along the c axis of the Δ-**2** crystal. In the present experiment, the XMCD signal was too weak to be detected, even under an applied magnetic field of 17 T (Fig. S11†). From the noise level in the XMCD spectra, we could only give an estimated upper limit of the signal, <0.2%, with respect to the edge jump. Whenever a crystal exhibits X-ray natural circular dichroism, the true XMCD signal can be obtained only as a combination of four X-ray absorption spectra measured independently (eqn (1)). In our case, the XMCD signal can be seen as the difference between two XNCD signals measured with opposite directions of applied magnetic field, $\sigma_{XMCD}(H) = \sigma_{XNCD}(H^+) - \sigma_{XNCD}(H^-)$. Since the crystals are chiral, both $\sigma_{XNCD}(H^+)$ and $\sigma_{XNCD}(H^-)$ are "large" with similar intensities, so one indeed expects the XMCD signal to be difficult to detect. On the other hand, the magnetic moment of Δ-**2** and Λ-**2** originating from the three metal–metal bonded cobalt atoms is quite small. Out of the 21 3d electrons, all are paired, except for one that lies in a highly delocalized SOMO with σ_{nb} symmetry.[11] With three cobalt atoms and a maximum magnetic moment of 1 μ_B, and no 3d density on the central cobalt atom due to symmetry reasons, each cobalt atom carries a maximum moment of 0.5 μ_B. In addition to the small average magnetic moment, DFT calculations on the parent dichloride derivative showed that the SOMO presents substantial density on the chlorine atoms, reducing even further the average magnetic polarization of the cobalt atoms.[12] This can be compared to more common situations where high-spin divalent cobalt atoms carry a spin magnetic moment of 3 μ_B with some additional orbital magnetic moment.[7b,20] When comparing with previous Co K-edge XMCD data from literature, e.g. Co^{2+} ions in a ZnO crystal, a simple cross-multiplication suggests that the expected intensity for XMCD in sample **2** cannot be larger than 2 × 10^{-4} of the XAS spectra.[20a] This small signal would already be quite difficult to measure in non-chiral crystals, but in the present case it is completely obscured by the presence of the XNCD signals that, as we will show, are as large as 2% of the XAS cross-sections.

In order to check for the absence of structural distortions in these crystals, we further performed X-ray Natural Linear Dichroism (XNLD) measurements (Fig. 4). In non-cubic crystals possessing a symmetry axis of an order larger or equal to three, the XNLD signal is measured by

$$\sigma_{XNLD} = \sigma_\perp - \sigma_\parallel$$

where $\sigma_\perp$ and $\sigma_\parallel$ are the cross-sections measured with the linear polarization vector ε perpendicular or parallel, respectively, to the symmetry axis. For such crystals, the main contribution comes from the electric dipole term and one usually neglects the electric quadrupole term. We first mounted a crystal of Λ-**2**
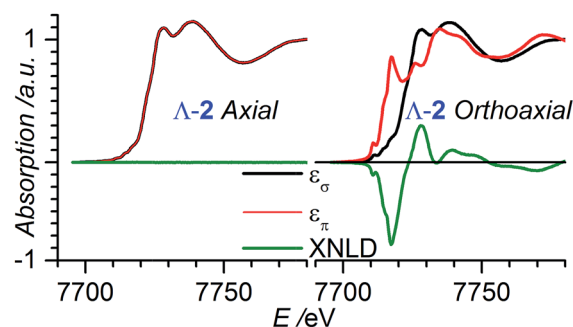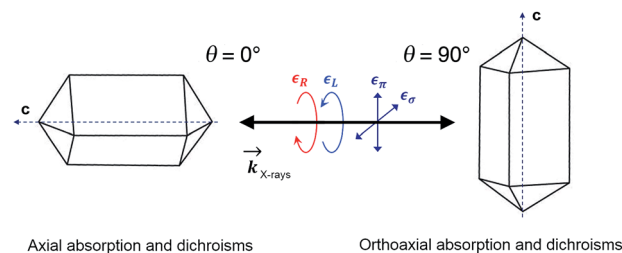

Fig. 4 XANES and XNLD obtained with linearly polarized X-rays for (a) axial ($\theta = 0°$) and (b) orthoaxial ($\theta = 90°$) configurations.

in the orthoaxial configuration, with the c axis perpendicular to the propagation vector of the X-rays (the $\theta = 90°$ geometry in Scheme 1), and recorded the spectra for two orthogonal linearly polarized X-rays, ε_π and ε_σ. In this experimental geometry, ε_π is parallel to the 4-fold axis, whereas ε_σ is perpendicular to it. A large XNLD signal, amounting to 70% of the XAS cross-section, was obtained (Fig. 4b). To further confirm the 4-fold axis symmetry, we mounted a crystal of Λ-**2** in axial configuration, with the 4-fold axis parallel to the X-ray propagation vector (the $\theta = 0°$ geometry in Scheme 1), and again recorded spectra with ε_π and ε_σ linear polarizations. Any distortion reducing the 4-fold axis to 2-fold would be detected by the presence of a difference signal in this geometry and Fig. 4a clearly shows the absence of such signal thus confirming the 4-fold symmetry of the crystal.

In order to verify that the crystals of Δ-**2** and Λ-**2** exhibit the expected chirality, we performed XNCD for several crystals of both enantiomers using circularly polarized X-rays (Fig. 5a). Whenever the spectra are recorded under an applied magnetic field or the sample has a finite magnetization, the true XNCD spectra should be calculated as a half-sum of the difference of the absorption spectra obtained with left and right circular polarizations for two directions of applied magnetic field (see eqn (3)). Since the XNCD is independent of magnetic field and our samples are not magnetically ordered, the true XNCD signal is given by $\sigma_L - \sigma_R$. Here the experiments were performed without an applied magnetic field and the XNCD spectra were calculated

Scheme 1 Schematic diagram of the measurement geometry showing the relationship between the tetragonal crystal axes and the direction and polarization of the X-ray beams. Axial geometry corresponds to the X-ray wavevector being parallel ($\theta = 0°$) to the crystal c axis whereas in the orthoaxial configuration the X-ray propagation direction is perpendicular to the optical axis of the crystal.
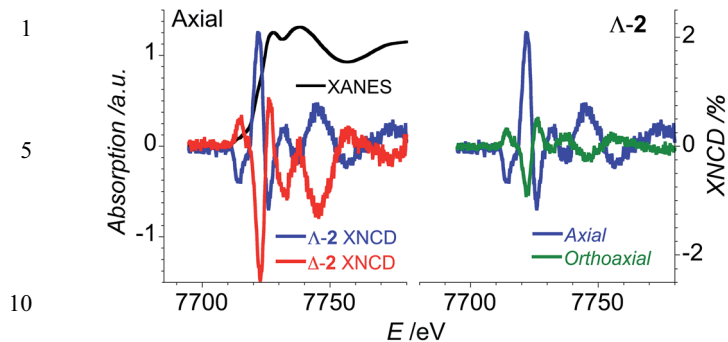
Fig. 5 (a) XANES (black) and XNCD spectra obtained in axial configuration ($\theta = 0°$) for Δ-**2** (red) and Λ-**2** (blue); (b) comparison axial (blue) and orthoaxial (green) XNCD spectra for a crystal of Λ-**2**.

as the difference of the absorption spectra obtained with left and right circular polarizations. As shown in Fig. 5a, with the crystal c axis mounted parallel to the incident X-ray beam ($\theta = 0°$), the cobalt enantiomers in Δ-**2** and Λ-**2** display the expected mutual mirror-image symmetry. The axial XNCD signals are rather large, with intensities up to about 2% of the absorption cross-section. Given that the intensity of the XNCD signals are equivalent for both enantiomers over several measured samples, we can conclude that the crystals are effectively enantiopure.

X-ray natural circular dichroism stems from the interference terms which mix multipole transitions of opposite parity: the electric dipole–electric quadrupole, *i.e.* 1 s → (p,d) in the case of the K-edge. As one can see from Fig. 5, the XNCD spectrum in **2** covers a wide energy range (more than 50 eV above the absorption edge), indicating that spatially extended d orbitals in the continuum hybridized with p-states of the Co atom also contribute, together with more localized 3d–4p orbitals.

As opposed to its analogue in the visible range, XNCD has a more complicated angular dependence and is observable only in 13 non-centrosymmetric crystal point groups. For the point group D_4, symmetry requires that the angular dependence of XNCD varies as a function of a single spectral shape, σ_{XNCD} multiplied by the angular factor $(3 \cos^2 \theta - 1)$, where θ is the polar angle between the crystal c axis, the optical axis, and the wave vector $k \rightarrow$.[21] This dependence can be indeed observed in the XNCD spectra when varying the θ angle (Fig. S12†), and is best observed by plotting the XNCD signals for axial $\theta = 0°$ and orthoaxial $\theta = 90°$ configurations (Fig. 5b) where one observes that $\sigma_{XNCD} (\theta = 90°) = -1/2 \, \sigma_{XNCD} (\theta = 0°)$, as expected for the angular dependence of $(3 \cos^2 \theta - 1)$ predicted by group theory.

Circularly polarized light is the 90° phase-shifted sum of vertical and perpendicular polarizations. When $\theta = 90°$, half of the circularly polarized X-rays is parallel to the crystalline c axis, and half is perpendicular. Accordingly, the XANES spectrum obtained with circularly polarized light is equivalent to the averaged spectra obtained from horizontal and vertical polarization (Fig. S13†). Conversely, when $\theta = 0°$, the circular polarization of X-rays is always perpendicular to the c axis and is thus equivalent to the case with $\theta = 90°$ under horizontal linear polarization (Fig. S13†).

In the XMCD experiments, all four spectra $\sigma_{H^+,L}$, $\sigma_{H^-,L}$, $\sigma_{H^+,R}$ and $\sigma_{H^-,R}$ have been recorded, and it is thus also possible to extract the X-ray magneto-chiral dichroism. It was however found that $\sigma_{XM\chi D}$ cannot be distinguished from the background noise (Fig. S11†). For XMχD to be present at the K-edge, one needs both a large orbital magnetic polarization of the absorbing atom and a strong p–d orbital hybridization. The p–d hybridization is present, as demonstrated by XNCD signal that is larger than 1% between the pre-edge feature up to 25 eV above the main rising edge. On the other hand, the rather small magnetic polarization that already precluded us from measuring a sizeable XMCD effect is very likely responsible for the absence of detectable magnetochiral effect.

Conclusions

We have used the chiral anion $[As_2(tartrate)_2]^{2-}$ to easily resolve racemic mixtures of $[Co_3(dpa)_4]^{2+}$ cations by selective crystallization. Both EMAC enantiomers crystallize as $[Co_3(dpa)_4-(MeCN)_2][(NBu_4)_2[As_2(tartrate)_2]_2$ in the non-centrosymmetric space group $P42_12$ with Flack parameters statistically equal to zero. The chiral EMACs display persistent optical activity in solution, as evidenced by mirror-image circular dichroism spectra in MeCN. Single crystals of $[Co_3(dpa)_4(MeCN)_2]-(NBu_4)_2[As_2(tartrate)_2]_2$ furthermore display substantial optical activity in the hard X-ray range, giving mirror-image X-ray natural circular dichroism at the cobalt K-edge. The angular dependence of the XNCD and XNLD spectra is consistent with what is expected for a system with D_4 symmetry. Unfortunately, the strongly delocalized nature of the magnetism in these systems did not allow us to record XMCD and XMχD signals even under an applied magnetic field of 17 T. Nonetheless, these results demonstrate that polarized X-rays provide an original approach for the investigation of chirality and symmetry in single crystals.

We are now examining the efficacy of our synthetic method for the separation of chiral EMACs with higher nuclearity and different metal centers (*e.g.* chromium, nickel and copper). With potentially higher specific rotation with increasing nuclearity, ground states with a larger magnetic moment, and catalytically active axial sites, chiral EMACs open interesting perspectives in non-linear optics, magneto-optical effects and asymmetric synthesis.

Experimental section

Materials and methods

All manipulations were carried out under dry nitrogen or argon using standard drybox or Schlenk techniques. Tetrahydrofuran, dichloromethane, diethyl ether and acetonitrile were purified using an Innovative Technologies solvent purification system. $CoCl_2$ was purchased from Fisher Chemicals and dried for several days at 130 °C before use. 2,2′-Dipyridylamine was purchased from Aldrich and recrystallized in hexane. $AgBF_4$ was purchased from stream and stored in a nitrogen glovebox. $[Co_3(dpa)_4Cl_2]$,[15] Δ-**1** and Λ-**1**[21] were prepared as reported elsewhere.

Synthesis

General synthesis for 2. $[Co_3(dpa)_4Cl_2]$ (0.15 g, 0.16 mmol) and $AgBF_4$ (0.07 g, 0.36 mmol) in 2 mL of CH_3CN were stirred at room temperature for 16 h. The resulting deep green solution was filtered using VWR plastic filter (0.2 μm) and a solution of Δ-**1** or Λ-**1** (0.16 g, 0.17 mmol) in 1 mL of MeCN was added. The solution was stirred for 1 h and the resulting solid was filtered off, dissolved in MeCN and recrystallized by ether vapor diffusion.

[Δ-Co$_3$(dpa)$_4$(MeCN)$_2$](NBu$_4$)$_2$[Λ-As$_2$(tartrate)$_2$]$_2$ solvent, Δ-2. Yield: 42% (0.16 g). Elemental analysis calc. for $C_{92}H_{118}As_4$-$Co_3N_{16}O_{24}(C_4H_{10}O)_{0.5}(H_2O)$ (2363.61 g mol^{-1}) C 47.77, H 5.33, N 9.48; found C 47.31, H 5.55, N 9.28. IR (ATR, cm^{-1}): 2273 w, 1657 s, 1606 s, 1592 s, 1548 w, 1471 s, 1457 s, 1426 s, 1371 m, 1314 m, 1283 w, 1265 w, 1155 s, 1125 s, 1071 m, 1023 s, 899 s, 840 m, 808 m, 761 m, 733 s, 661 m, 573 m.

[Λ-Co$_3$(dpa)$_4$(MeCN)$_2$](NBu$_4$)$_2$[Δ-As$_2$(tartrate)$_2$]$_2$ solvent, Λ-2. Yield: 41% (0.15 g). Elemental analysis calc. for $C_{92}H_{118}As_4$-$Co_3N_{16}O_{24}(C_4H_{10}O)_{0.5}$ (2345.59 g mol^{-1}) C 48.13, H 5.29, N 9.55; found C 48.18, H 5.53, N 9.22. IR (ATR, cm^{-1}): 2280 w, 1606 s, 1593 s, 1549 w, 1470 s, 1457 s, 1426 s, 1371 m, 1314 m, 1282 w, 1264 w, 1155 s, 1125 s, 1071 m, 1023 s, 900 s, 841 m, 807 m, 761 m, 732 s, 660 m, 573 m.

[Co$_3$(dpa)$_4$(MeCN)$_2$][As$_2$(tartrate)$_2$]·2MeCN, *rac*-3. $[Co_3$-$(dpa)_4Cl_2]$ (0.05 g, 0.05 mmol), $AgBF_4$ (0.02 g, 0.1 mmol) and 10 mL of CH_3CN were stirred at room temperature for 16 h to give a deep green solution and a white precipitate. The resulting solution was filtered using VWR plastic filter (0.2 μm) and a mixture of Δ-**1** (0.03 g, 0.03 mmol) and Λ-**1** (0.03 g, 0.03 mmol) was added. Overnight, large brown blocks were obtained. Yield 95% (0.07 g). Elemental analysis calc. for $C_{52}H_{42}As_2Co_3N_{14}$-$O_{12}(CH_3CN)_{0.25}(H_2O)_{1.35}$ (1416.22 g mol^{-1}) C 44.53, H 3.23, N 14.09; found C 44.79, H 3.50, N 13.85. IR (ATR, cm^{-1}): 2264 w, 1659 s, 1604 s, 1594 s, 1548 w, 1454 s, 1422 s, 1372 m, 1335 m, 1314 m, 1269 w, 1169 w, 1157 w, 1150 w, 1128 m, 1073 m, 1021 m, 920 w, 898 w, 885 w, 850 w, 840 w 806 m, 767 w, 757 m, 732 s, 659 w, 633 m, 572 w.

Physical measurements

CHNS elemental analyses were performed on a Flash EA1112 ThermoFisher Scientific at the ICMCB or by the Service d'Analyse Elementaire in Nancy. IR spectra were measured on a Nicolet 6700 FT-IR equipped with a SMART iTR™ accessory. Magnetic susceptibility measurements were obtained using a Quantum Design MPMS-XL SQUID magnetometer. The measurements were performed on a polycrystalline sample of Δ-**2** (35.9 mg) or Λ-**2** (16.7 mg) introduced in a polyethylene bag (3 × 0.5 × 0.02 cm). The dc measurements were conducted from 400 to 1.8 K at 0.1 and 1 T applied dc field. An *M vs. H* measurement was performed at 100 K to confirm the absence of ferromagnetic impurities. CD spectra in solution were obtained on a Jasco J-815 spectrophotometer. The measurements were made on samples with a 1.72 × 10^{-5} M and 1.62 × 10^{-5} M concentration for Δ-**2** and Λ-**2**, respectively. These samples were prepared by dissolving either 0.992 mg of Δ-**2** or 0.936 mg of Λ-**2** in 25 mL of MeCN. Class A volumetric flasks and a Mettler MX5 microbalance with an estimated weighting error of

2 μg were employed in the sample preparation. All spectra were measured with a scan speed of 50 nm min^{-1} and a 2 nm bandwidth. Data in millidegree were converted to the differential extinction coefficient ($\Delta\varepsilon$) using the equation:

$$\Delta\varepsilon = \frac{\theta}{32980 \times c \times l}$$

where θ is the measured CD ellipticity in millidegrees, c is the concentration in mol L^{-1}, and l is the pathlength of the cuvette in cm.

Crystallography

Crystals suitable for X-ray diffraction were selected under immersion oil in ambient conditions and attached to a MiTeGen microloop. The crystals were mounted in a stream of cold nitrogen at 120(2) K and centered in the X-ray beam using a video camera. Data collections were performed with Mo Kα (λ = 0.71073 Å) radiation on a Bruker Quazar SMART APEXII, operating at 50 kV and 30 mA using graphite monochromated radiation. The data were collected using a routine to survey reciprocal space, and reduction was performed using software included in Bruker Apex2 suite.[22] The structures were solved using direct methods.[23,24] Non-hydrogen atoms were refined anisotropically using weighted full-matrix least-squares on F^2, followed by difference Fourier synthesis.[25,26] All hydrogen atoms were included in the final structure factor calculation at idealized positions and were allowed to ride on the neighboring atoms with relative isotropic displacement coefficients. The Platon SQUEEZE routine[18] was used to account for diffuse electron density arising from interstitial solvent, which could not be modeled atomistically. Powder X-ray diffraction data were recorded using a PANalytical X'Pert PRO MPD diffractometer with Bragg–Brentano geometry, Cu-Kα radiation (λ = 1.54184 Å) and a graphite back scattering monochromator, using standard Al sample holders.

X-ray absorption

X-ray absorption experiments at the Co K-edge were carried out at the ID12 beamline of the European Synchrotron Radiation Facility (Grenoble, France), dedicated to polarization dependent X-ray spectroscopy in the 2–15 keV energy range. A high flux of circularly polarized photons was provided by an HELIOS-II undulator. X-rays were monochromatized by a Si ⟨111⟩ double crystal monochromator. Linearly polarized X-rays were obtained using a 0.9 mm thick diamond quarter wave plate inserted downstream with respect to the monochromator. For XNCD and XNLD studies, the samples were mounted on an aluminum sample holder and oriented so that the crystal's c axis and the photons wave vector formed an angle of 0° or 90°. All spectra were recorded at room temperature in total X-ray fluorescence yield detection mode in backscattering geometry. XNLD spectra were obtained by flipping the two orthogonal linear polarizations of the X-rays at every point of the energy scan. Each set of XNCD spectra were acquired by alternating the photon helicity after each spectrum 6 times, for a total of 12 absorption spectra.

XMCD and XMχD spectra were obtained by also using the total fluorescence yield detection mode in backscattering

geometry, but under an applied magnetic field. The samples were mounted on the cold finger of a constant-flow helium cryostat inserted in the bore of a superconducting solenoid producing a magnetic field up to 17 T. The temperature of the samples were kept at 3.1 K. Under these experimental conditions, the samples were magnetically saturated.

Conflicts of interest

There are no conflicts to declare.

Acknowledgements

References

1 (a) S.-A. Hua, M.-C. Cheng, C.-h. Chen and S.-M. Peng, *Eur. J. Inorg. Chem.*, 2015, 2510; (b) M. Majumdar and J. K. Bera, Supramolecular and Self-Assembled Metal-Containing Materials, in *Macromolecules Containing Metal and Metal-Like Elements*, ed. A. Abd-El Aziz, C. E. Carraher, C. U. Pittman and M.Zeldin, John Wiley & Sons, Inc., 2009, vol. 9, pp. 182–253; (c) J. F. Berry, in *Multiple Bonds between Metal Atoms*, ed. F. A. Cotton, C. A. Murillo and R. A. Walton, Springer U.S., 2005, pp. 669–706.

2 R. Clérac, F. A. Cotton, K. R. Dunbar, T. Lu, C. A. Murillo and X. Wang, *Inorg. Chem.*, 2000, **39**, 3065.

3 (a) D. W. Armstrong, F. A. Cotton, A. G. Petrovic, P. L. Polavarapu and M. M. Warnke, *Inorg. Chem.*, 2007, **46**, 1535; (b) M. M. Warnke, F. A. Cotton and D. W. Armstrong, *Chirality*, 2007, **19**, 179.

4 C.-H. Yu, M.-S. Kuo, C.-Y. Chuang, G.-H. Lee, S.-A. Hua, B.-Y. Jin and S.-M. Peng, *Chem.–Asian J.*, 2014, **9**, 3111.

5 R. A. Pascal Jr and A. P. West Jr, *Tetrahedron*, 2013, **69**, 6108.

6 (a) J. Goulon, C. Goulon-Ginet, A. Rogalev, V. Gotte, C. Malgrange, C. Brouder and C. R. Natoli, *J. Chem. Phys.*, 1998, **108**, 6394; (b) L. Alagna, T. Prosperi, S. Turchini, J. Goulon, A. Rogalev, C. Goulon-Ginet, C. R. Natoli, R. D. Peacock and B. Stewart, *Phys. Rev. Lett.*, 1998, **80**, 4799.

7 (a) B. Stewart, R. D. Peacock, L. Alagna, T. Prosperi, S. Turchini, J. Goulon, A. Rogalev and C. Goulon-Ginet, *J. Am. Chem. Soc.*, 1999, **121**, 10233; (b) R. Sessoli, M.-E. Boulon, A. Caneschi, M. Mannini, L. Poggini, F. Wilhelm and A. Rogalev, *Nat. Phys.*, 2015, **11**, 69; (c) I. Mihalcea, M. Perfetti, F. Pineider, L. Tesi, V. Mereacre, F. Wilhelm, A. Rogalev, C. E. Anson, A. K. Powell and R. Sessoli, *Inorg. Chem.*, 2016, **55**, 10068.

8 J. Goulon, C. Goulon-Ginet, A. Rogalev, G. Benayoun, C. Brouder and C. R. Natoli, *J. Synchrotron Radiat.*, 2000, **7**, 182.

9 J. Goulon, A. Rogalev, F. Wilhelm, C. Goulon-Ginet, P. Carra, D. Cabaret and C. Brouder, *Phys. Rev. Lett.*, 2002, **88**, 2374011.

10 R. Clérac, F. A. Cotton, L. M. Daniels, K. R. Dunbar, K. Kirschbaum, C. A. Murillo, A. A. Pinkerton, A. J. Schultz and X. Wang, *J. Am. Chem. Soc.*, 2000, **122**, 6226.

11 M.-M. Rohmer and M. Bénard, *J. Am. Chem. Soc.*, 1998, **120**, 9372.

12 M.-M. Rohmer, A. Strich, M. Bénard and J.-P. Malrieu, *J. Am. Chem. Soc.*, 2001, **123**, 9126.

13 D. Marcovich and R. E. Tapscott, *J. Am. Chem. Soc.*, 1980, **102**, 5712.

14 (a) S. Yamazaki and H. Yoneda, *Inorg. Nucl. Chem. Lett.*, 1979, **15**, 195; (b) H. Nakazawa and H. Yoneda, *J. Chromatogr.*, 1978, **160**, 89; (c) J. E. Harris, N. Desai, K. E. Seaver, R. T. Watson, N. A. Kane-Maguire and J. F. Wheeler, *J. Chromatogr. A*, 2001, **919**, 427.

15 (a) B. D. Sarma Jr and J. C. Bailar, *J. Am. Chem. Soc.*, 1955, **77**, 5480; (b) U. Sakaguchi, K. Tomioka, T. Kashihara and H. Yoneda, *Inorg. Chem.*, 1985, **24**, 463; (c) J. D. Harper, K. A. Kane-Maguire, L. A. P. Kane-Maguire and N. A. P. Kane-Maguire, *Inorg. Chim. Acta*, 1996, **249**, 5.

16 (a) A. Zalkin, D. H. Templeton and T. Ueki, *Inorg. Chem.*, 1973, **12**, 1641; (b) T. Bark, A. von Zelewsky, D. Rappoport, M. Neuburger, S. Schaffner, J. Lacour and J. Jodry, *Chem.–Eur. J.*, 2004, **10**, 4839; (c) K. Miyoshi, S. Izumoto, K. Nakai and H. Yoneda, *Inorg. Chem.*, 1986, **25**, 4654; (d) K. Miyoshi, S. Izumoto and H. Yoneda, *Bull. Chem. Soc. Jpn.*, 1986, **59**, 3475.

17 F. A. Cotton, L. M. Daniels and G. T. Jordan IV, *Chem. Commun.*, 1997, 421.

18 A. L. Spek, *Acta Crystallogr., Sect. C: Struct. Chem.*, 2015, **71**, 9.

19 A. Naim, Y. Bouhadja, M. Cortijo, E. Duverger-Nédellec, H. D. Flack, E. Freysz, P. Guionneau, A. Iazzolino, A. Ould Hamouda, P. Rosa, O. Stefańczyk, and M. Zeggar, submitted.

20 (a) V. Ney, B. Henne, J. Lumetzberger, F. Wilhelm, K. Ollefs, A. Rogalev, A. Kovacs, M. Kieschnick and A. Ney, *Phys. Rev. B*, 2016, **94**, 224405; (b) B. Henne, V. Ney, J. Lumetzberger, K. Ollefs, F. Wilhelm, A. Rogalev and A. Ney, *Phys. Rev. B*, 2017, **95**, 05446.

21 C. R. Natoli, C. Brouder, P. Sainctavit, J. Goulon, C. Goulon-Ginet and A. Rogalev, *Eur. Phys. J. B*, 1998, **4**, 1.

22 Bruker-AXS APEX2, *SADABS, and SAINT Software Reference Manuals*, Madison, Wisconsin, USA, 2009.

23 A. Altomare, M. C. Burla, M. Camalli, G. L. Cascarano, C. Giacovazzo, A. Guagliardi, A. G. G. Moliterni, G. Polidori and R. Spagna, *J. Appl. Crystallogr.*, 1999, **32**, 115.

24 G. M. Sheldrick, *Acta Crystallogr., Sect. A: Found. Crystallogr.*, 2008, **64**, 112.

25 O. V. Dolomanov, L. J. Bourhis, R. J. Gildea, J. A. K. Howard and H. Puschmann, *J. Appl. Crystallogr.*, 2009, **42**, 339.

26 L. J. Farrugia, *J. Appl. Crystallogr.*, 2012, **45**, 84.